NeuroImage: Clinical 18 (2018) 485–493

Contents lists available at ScienceDirect

NeuroImage: Clinical

journal homepage: www.elsevier.com/locate/ynicl

Combining viscoelasticity, diffusivity and volume of the hippocampus for the diagnosis of Alzheimer's disease based on magnetic resonance imaging

Lea M. Gerischer[a,b,d], Andreas Fehlner[c], Theresa Köbe[a,d], Kristin Prehn[a,d], Daria Antonenko[a,d,g], Ulrike Grittner[e], Jürgen Braun[f], Ingolf Sack[c], Agnes Flöel[a,d,g,*]

[a] Charité – Universitätsmedizin Berlin, corporate member of Freie Universität Berlin, Humboldt-Universität zu Berlin, and Berlin Institute of Health, Department of Neurology, Berlin, Germany
[b] Berlin Institute of Health (BIH), Berlin, Germany
[c] Charité – Universitätsmedizin Berlin, corporate member of Freie Universität Berlin, Humboldt-Universität zu Berlin, and Berlin Institute of Health, Department of Radiology, Berlin, Germany
[d] Charité – Universitätsmedizin Berlin, corporate member of Freie Universität Berlin, Humboldt-Universität zu Berlin, and Berlin Institute of Health, NeuroCure Clinical Research Center, Berlin, Germany
[e] Charité – Universitätsmedizin Berlin, corporate member of Freie Universität Berlin, Humboldt-Universität zu Berlin, and Berlin Institute of Health, Department for Biostatistics and Clinical Epidemiology, Berlin, Germany
[f] Charité – Universitätsmedizin Berlin, corporate member of Freie Universität Berlin, Humboldt-Universität zu Berlin, and Berlin Institute of Health, Institute of Medical Informatics, Berlin, Germany
[g] University Medicine Greifswald, Department of Neurology, Greifswald, Germany

ARTICLE INFO

Keywords:
Alzheimer's disease
MR elastography
Viscoelasticity
Diffusivity
Hippocampus
Hippocampal volume
ROC

ABSTRACT

Dementia due to Alzheimer's Disease (AD) is a neurodegenerative disease for which treatment strategies at an early stage are of great clinical importance. So far, there is still a lack of non-invasive diagnostic tools to sensitively detect AD in early stages and to predict individual disease progression. Magnetic resonance elastography (MRE) of the brain may be a promising novel tool. In this proof-of-concept study, we investigated whether multifrequency-MRE (MMRE) can detect differences in hippocampal stiffness between patients with clinical diagnosis of dementia due to AD and healthy controls (HC). Further, we analyzed if the combination of three MRI-derived parameters, i.e., hippocampal stiffness, hippocampal volume and mean diffusivity (MD), improves diagnostic accuracy.

Diagnostic criteria for probable dementia due to AD were in line with the NINCDS-ADRDA criteria and were verified through history-taking (patient and informant), neuropsychological testing, routine blood results and routine MRI to exclude other medical causes of a cognitive decline.

21 AD patients and 21 HC (median age 75 years) underwent MMRE and structural MRI, from which hippocampal volume and MD were calculated. From the MMRE-images maps of the magnitude $|G^*|$ and phase angle φ of the complex shear modulus were reconstructed using multifrequency inversion. Median values of $|G^*|$ and φ were extracted within three regions of interest (hippocampus, thalamus and whole brain white matter). To test the predictive value of the main outcome parameters, we performed receiver operating characteristic (ROC) curve analyses.

Hippocampal stiffness ($|G^*|$) and viscosity (φ) were significantly lower in the patient group (both $p < 0.001$). ROC curve analyses showed an area under the curve (AUC) for $|G^*|$ of 0.81 [95%CI 0.68–0.94]; with sensitivity 86%, specificity 67% for cutoff at $|G^*| = 980$ Pa) and for φ an AUC of 0.79 [95%CI 0.66–0.93]. In comparison, the AUC of MD and hippocampal volume were 0.83 [95%CI 0.71–0.95] and 0.86 [95%CI 0.74–0.97], respectively. A combined ROC curve of $|G^*|$, MD and hippocampal volume yielded a significantly improved AUC of 0.90 [95%CI 0.81–0.99].

In conclusion, we demonstrated reduced hippocampal stiffness and reduced hippocampal viscosity, as determined by MMRE, in patients with clinical diagnosis of dementia of the AD type. Diagnostic sensitivity was further improved by the combination with two other MRI-based hippocampal parameters. These findings motivate further investigation whether MMRE can detect decreased brain stiffness already in pre-dementia stages, and whether these changes predict cognitive decline.

* Corresponding author at: Department of Neurology, Universitätsmedizin Greifswald, Ferdinand Sauerbruch Strasse, 17475 Greifswald, Germany.
E-mail address: agnes.floeel@uni-greifswald.de (A. Flöel).

https://doi.org/10.1016/j.nicl.2017.12.023
Received 2 August 2017; Received in revised form 20 November 2017; Accepted 16 December 2017
Available online 20 December 2017
2213-1582/ © 2017 The Authors. Published by Elsevier Inc. This is an open access article under the CC BY-NC-ND license (http://creativecommons.org/licenses/BY-NC-ND/4.0/).

1. Introduction

Alzheimer's Disease (AD) is the most common cause of dementia (ADI, 2016; Cummings, 2004; Nagy et al., 1998; Sperling et al., 2011). Due to the predicted demographic changes in the population with an increasing proportion of elderly individuals, the number of patients affected by dementia and its precursor, mild cognitive impairment (MCI) due to AD, is expected to rise up dramatically over the next decades (ADI, 2016). Research for a more accurate and earlier diagnosis of AD, particularly in its preclinical stages (Sperling et al., 2011), is ongoing and will be the basis for the implementation of new and earlier treatment strategies.

The diagnosis of MCI or dementia due to AD is still based on clinical criteria. The main criterion is the presentation of cognitive decline typically including memory, language and visuospatial functions that is not explained by a major psychiatric disorder. For the diagnosis of dementia, this decline has to be severe enough to interfere with the individual's ability to perform activities of daily living (McKhann et al., 2011). To differentiate MCI or dementia due to AD from other forms of cognitive impairment, several biomarkers are available (McKhann et al., 2011). These biomarkers fall into two main categories: First, biomarkers denoting evidence of amyloid-beta (Aβ) protein deposition in the brain (low cerebrospinal fluid (CSF) $A\beta_{42}$ and positive amyloid-positron emission tomography (PET) imaging), and most likely yielding evidence of the AD specific pathophysiological process. The second category encompasses biomarkers that indicate the progressive neuronal degeneration that takes place in the brain, and is less AD-specific, including elevated CSF tau protein, decreased ^{18}fluorodeoxyglucose (FDG) uptake in FDG-PET and atrophy on structural MRI of the brain (McKhann et al., 2011). These biomarkers either expose the patient to radiation (PET imaging) or involve an invasive procedure (lumbar puncture for CSF analysis), and are thus not suited for repeated measurements.

Structural MRI is a non-invasive method, but whole brain atrophy as detected on routine scans develops rather late in the course of the disease and is therefore not useful to diagnose pre-dementia stages (Jack Jr et al., 2010). A more specific approach is the measurement of hippocampal atrophy, which can already be present in pre-dementia stages (Hampel et al., 2008). Since manual volumetry is time consuming and rater dependent, automated segmentation tools have been developed (de Flores et al., 2015; Hampel et al., 2008; Misra et al., 2009; Teipel et al., 2015). These tools have shown promising results within research settings but their broad implementation into clinical routine is still lacking (Dill et al., 2015; Fox et al., 2013; Lotjonen et al., 2011). Another important MRI method is diffusion tensor imaging (DTI), which assesses the restricted diffusion of water in tissue. DTI has predominantly been used for white matter tract integrity but recent studies have also demonstrated its potential for assessing the integrity of small gray-matter structures such as the hippocampus (Antonenko et al., 2016; Fellgiebel and Yakushev, 2011). In AD, DTI reveals microstructural alterations within the hippocampus by pathologically elevated mean diffusivity (MD) (Cherubini et al., 2010; Fellgiebel and Yakushev, 2011; Yakushev et al., 2010), but its role for the diagnosis of AD is not yet clear (Fellgiebel and Yakushev, 2011). In sum, despite advances in biomarker research over the past years, we still lack non-invasive diagnostic tools to sensitively detect the disease in early stages (Albert et al., 2011; Sperling et al., 2011), and to predict individual disease progression (Hampel et al., 2008).

Magnetic resonance elastography (MRE) of the brain is a promising new candidate among the non-invasive diagnostic methods (Muthupillai et al., 1995). MRE assesses tissue structure through its mechanical properties. In principle, shear waves are being introduced into the brain by an external mechanical vibration source (Green et al., 2008; Kruse et al., 2008; Sack et al., 2008). The image acquisition of the induced tissue deformation is then synchronized to the external vibration source. In this way, different time steps of the propagating waves are captured. Finally, the wave fields are mathematically inverted to calculate viscoelastic parameters (Fehlner et al., 2015). These derived viscoelastic parameters reflect the microstructural integrity of the neuronal-glial matrix (Sack et al., 2013). There are two main viscoelastic parameters that are both derived from the complex shear modulus G^*: the magnitude of the shear modulus ($|G^*|$) stands for the softness or elasticity of the tissue while the phase angle (φ) provides an indication of the viscous, i.e., damping properties of the tissue (Sack et al., 2008).

Previous studies have demonstrated the decrease of brain viscoelastic parameters due to physiological aging (Sack et al., 2009) and due to neurodegenerative (Lipp et al., 2013) and neuroinflammatory disorders (Fehlner et al., 2016; Schregel et al., 2012; Wuerfel et al., 2010). In dementia due to AD, MRE detected decreased overall brain stiffness (Murphy et al., 2011; Murphy et al., 2016). Similar results were found for behavioral variant fronto-temporal dementia, a much rarer form of dementia (Huston 3rd et al., 2016). However, pathology in AD is known to advance from specific regions, most notably the medial temporal lobe including the hippocampus (Braak and Braak, 1991b; Jack Jr et al., 2010). Whereas the deposition of amyloid-plaques starts in the temporal neocortex and entorhinal cortex, the hippocampus is known to show early tau aggregation (Braak et al., 2013). The importance of the hippocampus for memory encoding and retrieval and the association of structural integrity of the hippocampus and memory performance have been widely demonstrated (Squire and Zola-Morgan, 1991).

Fortunately, recent advances in MRE research including the introduction of multifrequency MRE (MMRE) now allow us to compute a higher resolution of the anatomical structures in the elasticity maps (two independent parameter maps of the magnitude ($|G^*|$) and the phase angle (φ)) and therefore enabled the analysis of the viscoelastic properties of smaller brain regions (Braun et al., 2014; Guo et al., 2013; Johnson et al., 2016).

In this proof-of concept study, we therefore investigated whether MMRE can detect differences in the elasticity of the hippocampus between patients with clinical diagnosis of dementia due to AD (as defined by the NINCDS-ADRDA criteria for probable dementia due to AD (McKhann et al., 1984; McKhann et al., 2011)) and healthy controls (HC). First, we aimed to ascertain that MMRE is capable of detecting differences in the elasticity of small brain regions such as the hippocampus. Second, we hypothesized that patients with clinical diagnosis of dementia due to AD show decreased hippocampal stiffness compared to HC. Finally, we asked if the combination of elasticity with two well-known MRI-derived parameters, i.e., hippocampal atrophy (measured as hippocampal volume) and microstructure (indicated by mean diffusivity of the hippocampus) would further improve diagnostic accuracy.

2. Methods

2.1. Patients and controls

Patients were recruited from the memory clinic of the Department of Neurology (Charité University Hospital, Berlin). All patients had been given a clinical diagnosis of dementia before entering the study and met the NINCDS-ADRDA criteria for probable dementia due to AD (McKhann et al., 1984; McKhann et al., 2011). The diagnostic procedure in our memory clinic comprises history-taking with the patient and a knowledgeable informant (mostly the spouse or other family member) and an objective cognitive assessment firstly through short “bedside” testing like the Mini-Mental State Examination (MMSE). Additionally, blood results (including electrolytes, blood count, kidney and liver parameters, TSH, vitamin B12 and folic acid levels) and brain imaging (either CT or MRI, but preferably MRI) are reviewed and the patient is then sent for neuropsychological testing by an experienced neuropsychologist. In our memory clinic a clinical diagnosis of probable dementia due to AD is given if the criteria outlined in the NIA guidelines from 2011 (McKhann et al., 2011) are fulfilled.

All patients who receive a diagnosis of probable dementia due to AD

are counseled to have a lumbar puncture performed, in order to exclude an inflammatory cause of the dementia and in order to detect amyloid- and tau-protein levels in the CSF. Amyloid-PET is not available within the clinical routine in our center. By definition, the detection of amyloid biomarkers is not necessary for establishing a clinical diagnosis of probable dementia due to AD and is not recommended for routine diagnostic purposes in the NIA guidelines from 2011 (McKhann et al., 2011).

All patients included in this study had undergone the above-described diagnostic process and for patients who had undergone a lumbar puncture, the results from the CSF analysis were considered. One patient had additionally undergone an amyloid-PET. For this patient the results from the PET-scan were considered. Lumbar punctures, CSF analyses or amyloid-PET were not performed for study-purposes only.

Healthy controls were recruited from the community via advertisement. They had no subjective cognitive impairments, scored at least 26 on the MMSE, and underwent a standardized medical interview and neurological examination. Exclusion criteria for both groups comprised severe medical, neurological or psychiatric disease (other than dementia in the patient group), major brain pathologies identified on MRI scans like territorial stroke or brain tumor and contraindications for undergoing MRI (such as claustrophobia or presence of an implanted pacemaker).

Given reports of age- and gender-related differences in elasticity measures of the brain (Sack et al., 2009; Sack et al., 2011), groups were matched for age and gender.

The participants signed written informed consent prior to study related procedures and received a small compensation for study participation. The study was approved by the Ethics Committee of the Charité University Hospital Berlin, Germany, and was conducted in accordance with the declaration of Helsinki.

2.2. Neuropsychological testing

Neuropsychological assessment for all participants included the MMSE as a screening measure (see above), followed by the German version of the Consortium to Establish a Registry for Alzheimer's Disease (CERAD) neuropsychological assessment battery in the extended version, the CERAD-Plus (see https://www.memoryclinic.ch/de/main-navigation/neuropsychologen/cerad-plus). The CERAD-Plus consists of the following subtests (in order of administration): 1) Verbal Fluency, 2) modified Boston-Naming-Test (BNT; maximum 15 points), 3) the MMSE (maximum score of 30), 4) Word-List-Learning (sum of three learning trials; maximum score of 30), 5) Figure-Construction (maximum score of 11), 6) Word-List-Recall (maximum score of 10), 7) Word-List-Recognition (maximum score of 10), and 8) Figure-Recall (maximum score of 11), 9) Trail-Making-Test A, 10) Trail-Making-Test B and 11) Phonemic Fluency. All subtests of the CERAD-Plus were administered according to standard procedures, except for the MMSE, which was taken from the screening procedures. Additionally we calculated a composite total CERAD score, as proposed by Chandler et al., by adding up the results of 6 subtests (Verbal Fluency, modified BNT, Word-List-Learning, Word-List-Recall, Word-List-Recognition and Figure-Construction) with a maximum score of 100, followed by a factor to correct for age, gender and education (Chandler et al., 2005).

2.3. MRI and MMRE protocol

Participants first underwent a structural MRI scan, followed by the MMRE sequence (3 T Siemens Trio MR-System) using a 12-channel head coil at the Berlin Center for Advanced Neuroimaging. The 3D structural scanning protocol consisted of T1-weighted magnetization prepared rapid gradient echo (MPRAGE) imaging (TR = 1900 ms, TE = 2.52 ms, 192 sagittal slices, voxel size = 1.0 × 1.0 × 1.0 mm^3, flip angle = 9°) and a diffusion-weighted spin-echo echo-planar imaging (EPI) sequence (TR = 7500 ms, TE = 86 ms, 61 axial slices, voxel size = 2.3 × 2.3 × 2.3 mm^3; 64 directions with a *b*-value of 1000 s/mm^2 and 10 with a *b*-value of 0 s/mm^2). An additional T2-weighted fluid attenuated inversion recovery (FLAIR) sequence was acquired in order to exclude structural abnormalities. The Structural Imaging protocol (MPRAGE, FLAIR and diffusion weighted imaging) lasted 20 min.

The MMRE were performed using a single-shot spin-echo EPI-based MRE sequence (Fehlner et al., 2015). The MMRE setting is described in detail in (Streitberger et al., 2016) and shown in Fig. 1. Full 3D wave fields were acquired at 7 mechanical frequencies (30 to 60 Hz, 5 Hz

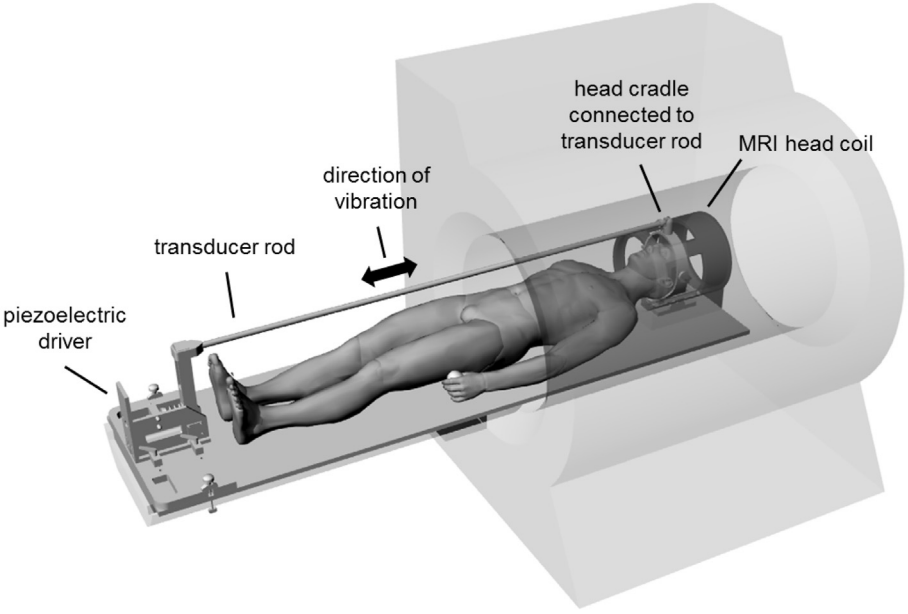

Fig. 1. MRE setup: A custom-designed nonmagnetic driver based on piezoelectric ceramics is mounted at the end of the patient table. The vibrations are transduced by a carbon fiber rod, which is connected to a custom-designed head cradle located inside the head coil. The vibrations induce a gentle nodding motion of the head.

increments) in 16 contiguous coronal slices and by an image resolution of $1.9 \times 1.9 \times 1.9\,mm^3$ (FoV: 190×160 mm, TR = 2980 ms, TE = 71 ms, 8 instances of the wave cycle). In total, we had an acquisition time of 7 min for a full MMRE protocol.

The total imaging time was 27 min. In between the structural scan and the MMRE, the participants had a short break in order to set up the MRE-head-cradle, where the participant would sit up and lay back down. They did not leave the scanner during this break. Overall, the scanning procedure was well tolerated by all 42 final participants of the study. Three Patients did not tolerate being in the scanner at all and were therefore excluded from the study.

2.4. Image processing

Analyses of the individual T1- and diffusion-weighted images (DTI) were performed with FSL (fsl version 4.1; http://www.fmrib.ox.ac.uk/fsl). The hippocampus volumes were segmented from the individual T1-structural images (FSL-FIRST, fsl version 4.1). Individual hippocampal volumes were adjusted to the total intracranial volume (TIV) according to previous studies (Raz et al., 2005) using the following formula: adjusted volume = raw volume – $b \times$ (TIV- mean TIV). The formula is based on the analysis of covariance approach and the coefficient b represents the slope of regression of a region of interest volume on TIV. Preprocessing of DTI data included eddy current and motion correction and extraction of non-brain tissue and was in line with previous studies (Kerti et al., 2013; Vernooij et al., 2009): Eddy current and head-motion correction were performed in FSL by means of an affine registration to the reference (b0) volume (Smith et al., 2004). The corrected data were skull-stripped by applying the FSL Brain Extraction Tool (Smith, 2002). Next, the tensor model was fitted to the diffusion data using the FMRIB Diffusion Toolbox (Behrens et al., 2003; Smith et al., 2004) to obtain individual 3D maps of mean diffusivity (MD). Images were inspected visually to identify and correct inaccurate brain extraction, registration or segmentation.

From the MMRE-images, we obtained two independent parameter maps of the elasticity measures by using an algorithm (multifrequency dual elasto-visco (MDEV) inversion) that was used in earlier studies (Braun et al., 2014; Fehlner et al., 2015; Guo et al., 2013; Hirsch et al., 2014; Streitberger et al., 2014). This algorithm implies frequency independence of the mechanical properties within the used frequency range in MMRE and provides two independent parameter maps of the magnitude ($|G^*|$) and the phase angle (φ) of the complex shear modulus G^*. As described above, $|G^*|$ provides an indication of the tissue elasticity and φ provides an indication of the damping properties or viscosity of the tissue (Sack et al., 2008). Both parameters are model-free and provide another representation of the storage and loss modulus in MRE. Additionally, a T2-weighted MRE magnitude image was generated, which was used for co-registration of the MRE-images with the high-resolution T1-image (MPRAGE).

We chose the hippocampus as region of interest (ROI) and the thalamus as reference region. The choice of reference structure was based on three criteria: First, the thalamus shows widespread neuropathological changes only in advanced stages of the disease (Braak and Braak, 1991b). Second, the thalamus as a deep gray matter structure can be segmented from the individual high-resolution T1-images (MPRAGE) using FSL-FIRST, and does not require manual delineation of a ROI. Third, our imaging technique with 16 contiguous coronal slices only permitted a limited choice of clearly defined brain structures that were fully included in the imaging zone.

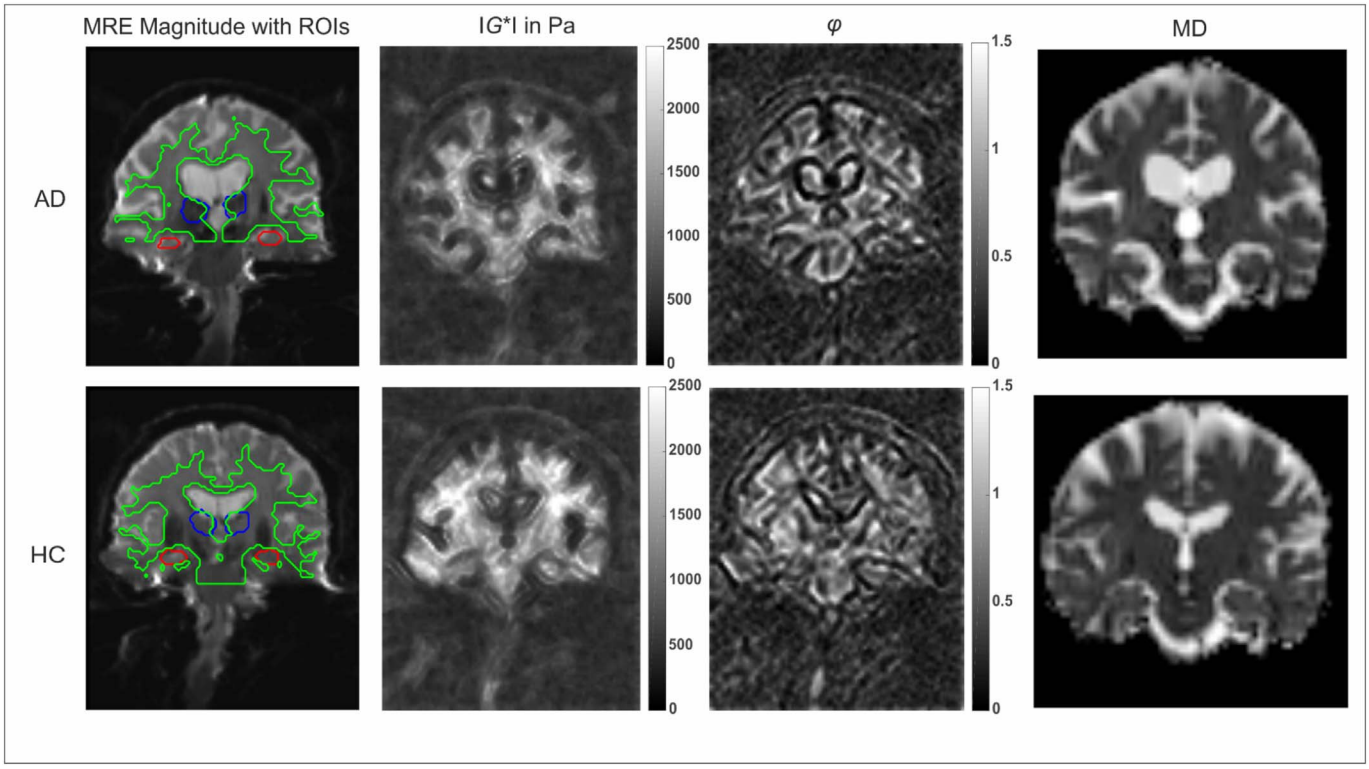

Fig. 2. The three regions of interest (ROIs) (green: whole brain white matter, blue: thalamus, red: hippocampus) are visualized at T2-weighted MRE magnitude images on the left. In the middle, two example parameter maps of $|G^*|$ in Pascal (Pa) and two example parameter maps of φ are visualized. On the right, two example maps of MD (mean diffusivity) are visualized, each for a patient (clinical diagnosis of dementia due to AD) (upper row) and a healthy control (HC) subject (lower row). AD: patients with clinical diagnosis of dementia due to Alzheimer's disease. $|G^*|$: magnitude of the shear modulus G^*. HC: healthy controls. MD: mean diffusivity. Pa: Pascal. φ: phase angle (dimensionless). (For interpretation of the references to color in this figure legend, the reader is referred to the web version of this article.)

Both regions were segmented from the individual T1-structural images (FSL-FIRST, fsl version 4.1) and then co-registered to the native space elasticity parameter maps (FSL-FLIRT). The segmented regions were used as masks for the elasticity and viscosity parameter maps $|G^*|$ and φ. Additionally, we generated a whole brain white matter (WM) mask (see Fig. 2). Within all masks median values were extracted.

2.5. Statistical analysis

Group characteristics were compared using independent *t*-tests for parametric variables, chi-square tests for binary variables and non-parametric tests if data were not sufficiently normally distributed (no unimodal distribution or $|\text{skewness}| > 1$).

The discriminative properties of the four measures: $|G^*|$, φ, MD and volume in the hippocampus, were calculated using receiver operating characteristics (ROC) analyses. We estimated the area under the ROC curve (AUC) with 95% confidence intervals. From the ROC curve of $|G^*|$ an optimal cutoff was visually defined to calculate sensitivity and specificity as well as the positive and negative predictive values. In a secondary analysis, we compared the ROC curves of the single variables and generated ROC curves of combinations of different measures (STATA version 13.1). Paired sample statistical techniques were used for the comparison of two biomarkers. The method exploits the mathematical equivalence of the AUC to the Mann-Whitney U-statistic (DeLong et al., 1988). For testing models with more than one marker against models using only one marker, we used a likelihood-ratio-test.

To analyse the relationship between elasticity and diffusivity we performed bivariate correlation analyses and reported the Pearson coefficient r. For all analyses, a two-tailed significance level of $\alpha = 0.05$ was considered. For this proof-of-concept study in which the association of viscoelastic measures of the hippocampus with a clinical diagnosis of Alzheimer's disease was analyzed for the first time, no adjustment for multiple testing was applied.

Statistical analyses were performed using IBM SPSS Statistics 22 and STATA version 13.1.

3. Results

3.1. Demographic characteristics

21 patients with clinical diagnosis of dementia due to AD and 21 HC participated in the study. Demographical data and clinical scores of both groups are shown in Table 1. Groups were comparable with regard to age, gender and years of education. As expected the two groups differed in their MMSE score.

In the patient group, clinical diagnosis of dementia due to AD had been established for an average of about two years. In 18 of 21 patients, information about CSF-analysis was available. One patient underwent an additional amyloid-PET and was found to be positive for amyloid-pathology on the PET-scan after previously having had negative results in CSF. An overview of the biomarker distribution is shown in Table 2.

As expected the groups differed in their results on the composite total CERAD score and in their results of the individual subtests of the CERAD-Plus neuropsychological assessment battery. An overview of the results is shown in Supplementary Table I.

Table 1
Demographical data, clinical scores.

	AD (N = 21)	HC (N = 21)
Age (yrs)	74 [67–80]	75 [66–79]
Female	10 (48%)	10 (48%)
Yrs of education	14 ± 3	15 ± 3
MMSE (points)	20 [16–22]	29 [28–30]
Yrs since diagnosis	2 ± 1	–

Data are median [IQR], mean ± SD or number (%); AD: patients with clinical diagnosis of dementia due to Alzheimer's Disease; HC: healthy controls; yrs.: years; MMSE: Mini Mental State Examination.

Table 2
Biomarkers for patient group.

	AD (N = 21)
CSF available	18 (86%)
CSF normal (tau & Aβ)	6 (28%)
Low Aβ (ratio[a])	10 (48%)
Only raised tau	2 (10%)
Additional amyloid-PET done	1[b] (5%)
Amyloid-PET positive	1 (5%)
Presence of Aβ-pathology (CSF + PET)	11 (52%)

Data are number (%); Aβ: beta-amyloid protein; a ratio below 0.40 is considered pathological. AD: patients with clinical diagnosis of dementia due to Alzheimer's Disease; CSF: Cerebrospinal fluid; PET: Positron Emission Tomography.

[a] Aβ ratio: ratio of Aβ1-42 × 10/Aβ1-40.

[b] One patient underwent amyloid-PET after being Aβ-negative in CSF (independent of the conduction of this study).

3.2. Mechanical properties (elasticity and viscosity)

In the patient group, $|G^*|$- and φ-values in the hippocampus ROI were significantly lower than in the HC group. For the thalamus, we observed comparable $|G^*|$- values between the two groups, but significantly lower φ-values in the patient group. Within the whole brain WM mask we observed both significantly lower $|G^*|$- and φ-values in the patient group (see Table 3). Fig. 3 visualizes the group results of $|G^*|$ in the three regions using boxplots.

To test the stability of the extracted values of $|G^*|$ and φ, we performed control analyses with slightly larger and slightly smaller ROIs for the three regions (hippocampus, thalamus, whole brain white matter ROI). For this, we enlarged and eroded the ROIs by one and by two voxels in the three dimensions. This did not change the results shown in Fig. 3 with regard to differences between the groups (data not shown).

Table 3
Main outcome parameters of elasticity and viscosity.

	AD (N = 21)	HC (N = 21)	p
$\|G^*\|$ of hippocampus (in Pa)	863 ± 147	1076 ± 190	< 0.001[a]
φ of hippocampus	0.43 ± 0.06	0.51 ± 0.07	< 0.001[a]
$\|G^*\|$ of thalamus (in Pa)	1208 ± 251	1283 ± 203	0.293[a]
φ of thalamus	0.65 ± 0.11	0.71 ± 0.08	0.043[a]
$\|G^*\|$ of WM (whole brain) (in Pa)	1387 ± 159	1544 ± 129	0.001[a]
φ of WM (whole brain)	0.59 ± 0.05	0.63 ± 0.05	0.007[a]

AD: patients with clinical diagnosis of dementia due to Alzheimer's disease, HC: healthy controls, $|G^*|$: magnitude of the complex shear modulus G*, φ: phase angle, Pa: Pascal, WM: white matter; values are given as mean ± SD.

[a] Independent *t*-test.

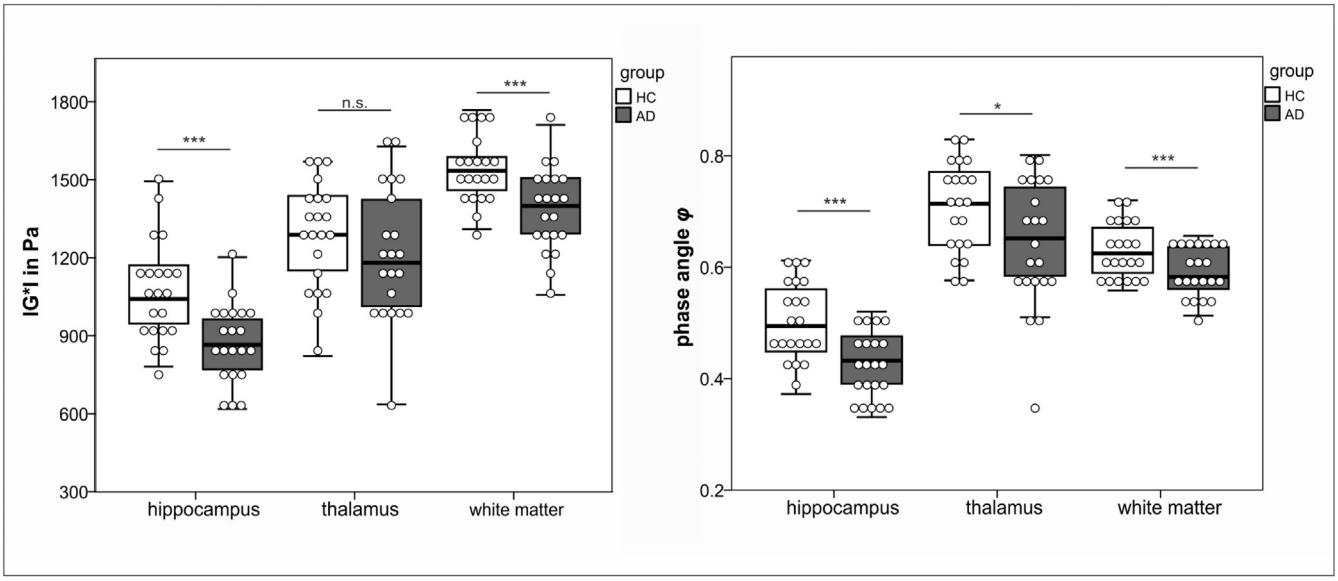

Fig. 3. Boxplots of $|G^*|$ and φ of the three regions with overlaid dotplot of the raw data: hippocampus, thalamus and whole brain white matter according to the high-resolution MDEV inversion. N = 21 in each group. AD: patients with clinical diagnosis of dementia due to Alzheimer's disease. HC: healthy controls. Pa: Pascal. |G*|: magnitude of the shear modulus G^*. φ: phase angle (dimensionless).

3.3. Hippocampal diffusivity and volume

MD was significantly higher in the patient group indicating a loss of integrity of tissue microstructure. Comparison of hippocampal volumes between groups revealed significantly smaller hippocampal volumes in the patient group (see Table 4).

Table 4
Diffusivity and volume of hippocampus.

	AD (N = 21)	HC (N = 21)	p
MD ($\times 10^{-3}$ mm^2/s)	1.31 ± 0.23	1.13 ± 0.09	0.003[a]
Volume ($\times 10^3$ mm^3)	2.83 ± 0.51	3.53 ± 0.40	< 0.001[a]

AD: Patients with clinical diagnosis of dementia due to Alzheimer's disease, HC: healthy controls, MD: mean diffusivity, values are given as mean ± SD.
[a] Independent t-test.

3.4. Comparison of elasticity, diffusivity and volume

To test the discriminative value of $|G^*|$ in the hippocampus for the distinction between the HC versus the patient group, we plotted the ROC curve (Fig. 4a), which yielded an AUC of 0.81 [95%CI 0.68–0.94]. From the ROC curve and the output table we determined a cutoff with a sensitivity not lower than 80% and corresponding highest possible specificity. That yielded a cut-point of $|G^*|$ = 980 Pa and corresponds to a sensitivity of 86% and a specificity of 67%. The positive predictive value was 72% and the negative predictive value was 82%.

We also plotted the ROC curve for φ, which yielded an AUC of 0.79 [95%CI 0.66–0.93]. Then we generated a combined ROC curve of $|G^*|$ and φ with an AUC of 0.83 [95%CI 0.70–0.95] and compared this to $|G^*|$ and φ alone using a likelihood ratio test (graphs not shown). The combined AUC did not perform better than either parameter alone (compared to $|G^*|$ alone $p = 0.243$; compared to φ alone $p = 0.104$). Given that the combination of $|G^*|$ and φ did not improve the discriminative value compared to using $|G^*|$ alone, only the $|G^*|$-properties of the hippocampus were considered in subsequent analyses.

The AUC values of $|G^*|$, volume and MD in the hippocampus were all > 0.8 (see Fig. 4). Combining these three variables ($|G^*|$, MD and volume) into one ROC curve further improved the AUC value to 0.90 [95%CI 0.81–0.99]. This value was significantly higher than $|G^*|$ only ($p = 0.005$), MD only ($p = 0.020$), or volume only ($p = 0.043$) using a likelihood ratio test.

Additionally, we performed correlation analyses for the relationship between elasticity and viscosity of the hippocampus with MD of the hippocampus. The scatterplots are shown in the Supplementary Fig. II. We found an inverse correlation for both viscoelastic measures with a lower elasticity or viscosity of the hippocampus correlating with a higher mean diffusivity.

3.5. Subgroup analysis by amyloid-pathology

Within our group of patients with dementia, 11 had proven Aβ-pathology (CSF or PET), whereas 7 had normal amyloid-levels in CSF and 3 patients did not receive any diagnostics in search of Aβ-pathology. We therefore performed subgroup analyses comparing the Aβ-positive subgroup with the rest of the AD patients. We found no significant differences between the subgroups with regard to age, gender, MMSE, years since diagnosis, or $|G^*|$, MD and volume of the hippocampus. This result did not change after excluding the 3 patients without any diagnostic procedure (data not shown). We additionally conducted an analysis comparing only the group of Aβ-positive patients with healthy controls. This did not change the results for the differences in elasticity measures within the hippocampus between the two groups (data not shown). Correlation analyses between CSF amyloid-β and elasticity of the hippocampus and between CSF amyloid-β and elasticity of the whole brain white matter mask did not show any significant correlations (all Pearson r's < 0.3).

4. Discussion

With this proof-of-concept study, we were able to show that MMRE is capable of detecting differences in the elasticity of small brain regions such as the hippocampus between patients with dementia, regardless of amyloid status, and HC. Moreover, we demonstrated that stiffness within the hippocampus, determined using MMRE, is lower in patients with clinical diagnosis of dementia of the AD type than in HC. Plotting the ROC curve for $|G^*|$of the hippocampus yielded a sensitivity of 86% and a specificity of 67% (cutoff at $|G^*|$ = 980 Pa). These values were

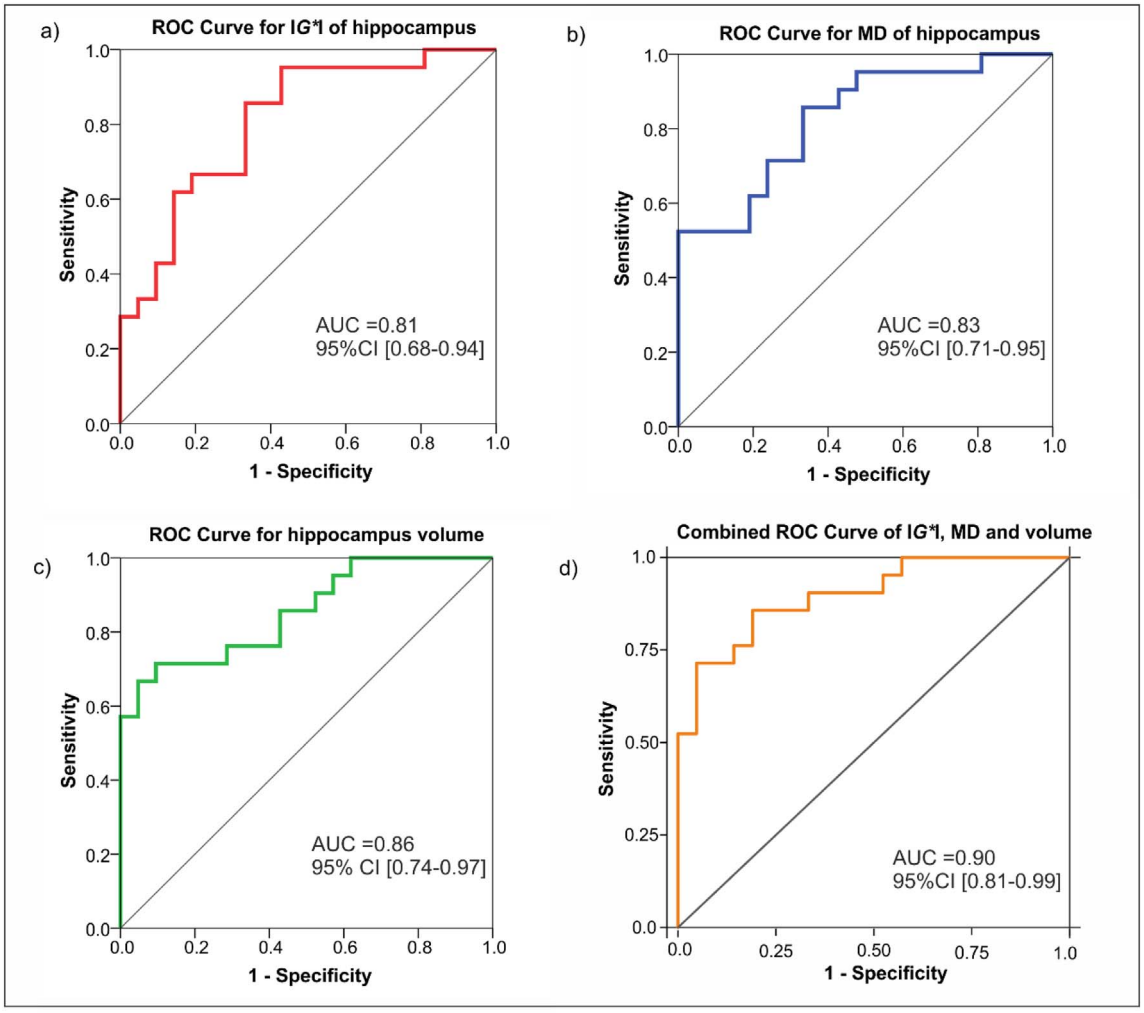

Fig. 4. Individual ROC curves for a) $|G^*|$, b) MD, c) volume of the hippocampus and d) combined ROC-curve of $|G^*|$, MD and volume. ROC: receiver operating characteristic. AUC: Area under (ROC) curve. CI: 95% confidence interval. $|G^*|$: magnitude of the complex shear modulus G^*. MD: mean diffusivity.

lower than those of amyloid-specific but invasive methods such as CSF analyses or amyloid-PET (best CSF parameter (CSF Aβ42/total tau) with 97% sensitivity and 83% specificity; amyloid-PET composite score with 85% sensitivity and 87% specificity (Palmqvist et al., 2015)). Finally, we demonstrated that the diagnostic sensitivity of our non-invasive approach was further improved by combining hippocampal stiffness with two other MRI-based hippocampal parameters, i.e., hippocampal volume and mean diffusivity; yielding a significantly higher AUC than either of the three parameters alone.

Similar to other studies (Murphy et al., 2011; Murphy et al., 2016), patients showed reduced stiffness within a whole brain white matter mask, indicating widespread neurodegenerative brain tissue changes due to the disease. However, our finding that stiffness within the thalamus, a gray matter brain region known to be affected late in the course of AD (Braak and Braak, 1991b), did not show clear differences between the groups, emphasizes the specificity of the MRE findings for degeneration patterns typical for AD (Braak and Braak, 1991b; Jack Jr et al., 2010).

Studies with MRE in mice, using a murine model of Parkinson's Disease, have demonstrated an association between the number of neurons in a brain region and its stiffness, indicating that a loss of neurons would lead to decreased stiffness (Hain et al., 2016; Klein et al., 2014). One study with a murine model of Alzheimer's disease found an overall decreased brain stiffness compared to wildtype mice (Murphy et al., 2012). Munder et al. (2018) showed an age-dependent cell loss in the hippocampus of AD mice that correlated with reduced stiffness. However there was no analysis that correlated stiffness changes with amyloid deposition. As the deposition of amyloid-plaques precedes neuronal loss and atrophy (Braak and Braak, 1997; Cummings, 2004), future studies in murine Alzheimer-models should investigate whether amyloid deposition alone already causes a measurable change in regional brain stiffness. To date, it remains unclear if stiffness changes are mainly due to deposition of amyloid-plaques in the AD brain, or if reduced stiffness is indicative for tau-pathology, neuronal loss, or inflammatory processes in the course of the disease (Ferreira et al., 2014; Heneka et al., 2015; Holmes, 2013). Our finding that stiffness did not differ between Aβ-positive patients with dementia and Aβ-negative patients with dementia would suggest that Aβ-pathology is less important for stiffness changes than other factors such as tau-pathology, neuronal loss, and/or inflammation. This hypothesis should be tested in animal models.

Finally, we were interested in comparing, and subsequently combining, the new parameter of hippocampal stiffness with two more widely employed MRI-derived parameters, i.e., hippocampal volume and microstructure (as determined by mean diffusivity).

As shown in Fig. 4, the ROC curve analyses demonstrated a comparable performance as predictive diagnostic test between the new parameter of hippocampal stiffness and the established MRI-derived parameters of hippocampal volume and diffusivity. The combined ROC curve of hippocampal stiffness, volume and mean diffusivity significantly improved prediction compared to the predictive values achieved by either of the three parameters alone. Since all three

parameters require one single MRI only, their combination may constitute a promising approach, not only for diagnosis but also for predicting conversion to dementia in early stages of AD, a hypothesis to be evaluated in future studies.

Further, the absolute difference in stiffness and volume was approximately 20% between patients and HC compared to only approximately 10% difference in diffusivity (see Tables 3 and 4). However, volumetry is highly dependent on the precision of hippocampal segmentation (de Flores et al., 2015; Dill et al., 2015; Hampel et al., 2008) and this might influence its reliability as imaging marker in follow-up examinations. The diagnostic accuracy of hippocampal MMRE was not influenced by the size of the ROI in the present study. We therefore expect MMRE to play an increasing role in MRI-based AD assessment in the future, in particular when ongoing technical improvements of wave stimulation and inversion methods are translated into a higher consistency of values.

The main limitation of this study is the small number of subjects investigated in each group. Therefore, the present results should be replicated in studies with larger samples. Also it would be desirable to confirm or refute amyloid-pathology (either in CSF or by amyloid-PET) in all individuals within the patient group. We addressed this uncertainty by performing subgroup analyses, comparing the Aβ-positive subgroup with the Aβ-negative subgroup, which allowed for conclusions towards underlying pathology, and additionally performing analyses with and without the patients for whom no information on amyloid- pathology was available. This did not change the main results of the study. Further, since the resolution of the MRE images was 1.9 mm cubic voxels, partial-volume effects might occur that affect the precision of the ROIs especially in a small region like the hippocampus (Salminen et al., 2016). Therefore, we performed additional analyses with eroded ROIs, which did not change the results. Future studies might technically address this issue by improving resolution of the MRE images. Unlike MD measurement, MRE parameter maps were not corrected for eddy currents and motions. EPI-based MRE is susceptible to field distortions near air-tissue interfaces which should be corrected as recently proposed by Fehlner et al. (2017). This method will be implemented in future MMRE studies to increase the spatial reliability of voxel-wise stiffness analysis.

Due to the choice of our imaging technique using coronal slices for the MRE, we were limited in analyzing further brain structures and chose the thalamus as reference structure even though studies by Braak and Braak found that parts of the thalamus are involved in neuropathological changes during AD starting in stage 2 (Braak and Braak, 1991a). This means that the thalamus is not a reference structure in the sense that it is not involved in AD pathology at all; rather, it shows involvement in the pathophysiological process in more advanced stages, and we therefore expected to find less difference in viscoelastic measures between healthy subjects and patients for the thalamus than for the hippocampus.

5. Conclusions and outlook

Since the hippocampus is targeted in the neurodegenerative process of AD early on (Braak and Braak, 1991b; Jack Jr et al., 2010), detection of decreased hippocampal stiffness may be a promising noninvasive biomarker for early diagnosis and progression monitoring in the future. Given previous histological findings in animal models, and the present results demonstrating that hippocampal stiffness did not differ between Aβ-positive and Aβ-negative patients with dementia, stiffness may be a sensitive marker for tau-pathology, neuronal loss, and/or inflammation, but not amyloid-pathology. This hypothesis is supported by the fact that tau-pathology, rather than amyloid-pathology, starts in the hippocampus (Braak et al., 2013). Future studies should evaluate an area known to harbor early amyloid-pathology, like the posterior cingulum/precuneus or the entorhinal cortex, to determine whether differences in amyloid-positive versus amyloid-negative patients can be detected by MMRE.

The results of this study motivate further investigation whether MMRE can detect decreased brain stiffness in early stages of the disease, and whether these changes predict clinical decline. To answer these questions, longitudinal studies in pre-dementia stages of AD would be most suitable.

Disclosures

The authors declare that they have no conflicts of interest.

Acknowledgments

Dr. Gerischer is participant in the BIH Charité Clinician Scientist Program funded by the Charité – Universitätsmedizin Berlin and the Berlin Institute of Health. Dr. Fehlner acknowledges a scholarship of the Hanns Seidel Foundation. This work was supported by grants from the Deutsche Forschungsgemeinschaft (Fl 379-10/1; Fl 379-11/1, DFG-Exc 257 and DFG-Sa901/17) and the Bundesministerium für Bildung und Forschung (FKZ 0315673A, 01EO0801, 01GQ1424A, 01GQ1420B, 01GQ1408).

Appendix A. Supplementary data

Supplementary data to this article can be found online at https://doi.org/10.1016/j.nicl.2017.12.023.

References

ADI, 2016. Alzheimer's Disease International: World Alzheimer Report 2016. https://www.alz.co.uk/research/WorldAlzheimerReport2016.pdf.

Albert, M.S., DeKosky, S.T., Dickson, D., Dubois, B., Feldman, H.H., Fox, N.C., Gamst, A., Holtzman, D.M., Jagust, W.J., Petersen, R.C., Snyder, P.J., Carrillo, M.C., Thies, B., Phelps, C.H., 2011. The diagnosis of mild cognitive impairment due to Alzheimer's disease: recommendations from the National Institute on Aging-Alzheimer's Association workgroups on diagnostic guidelines for Alzheimer's disease. Alzheimers Dement. 7, 270–279.

Antonenko, D., Kulzow, N., Cesarz, M.E., Schindler, K., Grittner, U., Floel, A., 2016. Hippocampal pathway plasticity is associated with the ability to form novel memories in older adults. Front. Aging Neurosci. 8, 61.

Behrens, T.E., Woolrich, M.W., Jenkinson, M., Johansen-Berg, H., Nunes, R.G., Clare, S., Matthews, P.M., Brady, J.M., Smith, S.M., 2003. Characterization and propagation of uncertainty in diffusion-weighted MR imaging. Magn. Reson. Med. 50, 1077–1088.

Braak, H., Braak, E., 1991a. Alzheimer's disease affects limbic nuclei of the thalamus. Acta Neuropathol. 81, 261–268.

Braak, H., Braak, E., 1991b. Neuropathological staging of Alzheimer-related changes. Acta Neuropathol. 82, 239–259.

Braak, H., Braak, E., 1997. Staging of Alzheimer-related cortical destruction. Int. Psychogeriatr. 9 (Suppl. 1), 257–261 (discussion 269-272).

Braak, H., Zetterberg, H., Del Tredici, K., Blennow, K., 2013. Intraneuronal tau aggregation precedes diffuse plaque deposition, but amyloid-beta changes occur before increases of tau in cerebrospinal fluid. Acta Neuropathol. 126, 631–641.

Braun, J., Guo, J., Lutzkendorf, R., Stadler, J., Papazoglou, S., Hirsch, S., Sack, I., Bernarding, J., 2014. High-resolution mechanical imaging of the human brain by three-dimensional multifrequency magnetic resonance elastography at 7T. NeuroImage 90, 308–314.

Chandler, M.J., Lacritz, L.H., Hynan, L.S., Barnard, H.D., Allen, G., Deschner, M., Weiner, M.F., Cullum, C.M., 2005. A total score for the CERAD neuropsychological battery. Neurology 65, 102–106.

Cherubini, A., Peran, P., Spoletini, I., Di Paola, M., Di Iulio, F., Hagberg, G.E., Sancesario, G., Gianni, W., Bossu, P., Caltagirone, C., Sabatini, U., Spalletta, G., 2010. Combined volumetry and DTI in subcortical structures of mild cognitive impairment and Alzheimer's disease patients. J. Alzheimers Dis. 19, 1273–1282.

Cummings, J.L., 2004. Alzheimer's disease. N. Engl. J. Med. 351, 56–67.

DeLong, E.R., DeLong, D.M., Clarke-Pearson, D.L., 1988. Comparing the areas under two or more correlated receiver operating characteristic curves: a nonparametric approach. Biometrics 44, 837–845.

Dill, V., Franco, A.R., Pinho, M.S., 2015. Automated methods for hippocampus segmentation: the evolution and a review of the state of the art. Neuroinformatics 13, 133–150.

Fehlner, A., Papazoglou, S., McGarry, M.D., Paulsen, K.D., Guo, J., Streitberger, K.J., Hirsch, S., Braun, J., Sack, I., 2015. Cerebral multifrequency MR elastography by remote excitation of intracranial shear waves. NMR Biomed. 28, 1426–1432.

Fehlner, A., Behrens, J.R., Streitberger, K.J., Papazoglou, S., Braun, J., Bellmann-Strobl, J., Ruprecht, K., Paul, F., Wurfel, J., Sack, I., 2016. Higher-resolution MR elastography reveals early mechanical signatures of neuroinflammation in patients with clinically isolated syndrome. J. Magn. Reson. Imaging 44, 51–58.

Fehlner, A., Hirsch, S., Weygandt, M., Christophel, T., Barnhill, E., Kadobianskyi, M., Braun, J., Bernarding, J., Lutzkendorf, R., Sack, I., Hetzer, S., 2017. Increasing the spatial resolution and sensitivity of magnetic resonance elastography by correcting for subject motion and susceptibility-induced image distortions. J. Magn. Reson. Imaging 46, 134–141.
Fellgiebel, A., Yakushev, I., 2011. Diffusion tensor imaging of the hippocampus in MCI and early Alzheimer's disease. J. Alzheimers Dis. 26 (Suppl. 3), 257–262.
Ferreira, S.T., Clarke, J.R., Bomfim, T.R., De Felice, F.G., 2014. Inflammation, defective insulin signaling, and neuronal dysfunction in Alzheimer's disease. Alzheimers Dement. 10, S76–83.
de Flores, R., La Joie, R., Chetelat, G., 2015. Structural imaging of hippocampal subfields in healthy aging and Alzheimer's disease. Neuroscience 309, 29–50.
Fox, C., Lafortune, L., Boustani, M., Dening, T., Rait, G., Brayne, C., 2013. Screening for dementia–is it a no brainer? Int. J. Clin. Pract. 67, 1076–1080.
Green, M.A., Bilston, L.E., Sinkus, R., 2008. In vivo brain viscoelastic properties measured by magnetic resonance elastography. NMR Biomed. 21, 755–764.
Guo, J., Hirsch, S., Fehlner, A., Papazoglou, S., Scheel, M., Braun, J., Sack, I., 2013. Towards an elastographic atlas of brain anatomy. PLoS One 8, e71807.
Hain, E.G., Klein, C., Munder, T., Braun, J., Riek, K., Mueller, S., Sack, I., Steiner, B., 2016. Dopaminergic neurodegeneration in the mouse is associated with decrease of viscoelasticity of substantia Nigra tissue. PLoS One 11, e0161179.
Hampel, H., Burger, K., Teipel, S.J., Bokde, A.L., Zetterberg, H., Blennow, K., 2008. Core candidate neurochemical and imaging biomarkers of Alzheimer's disease. Alzheimers Dement. 4, 38–48.
Heneka, M.T., Carson, M.J., El Khoury, J., Landreth, G.E., Brosseron, F., Feinstein, D.L., Jacobs, A.H., Wyss-Coray, T., Vitorica, J., Ransohoff, R.M., Herrup, K., Frautschy, S.A., Finsen, B., Brown, G.C., Verkhratsky, A., Yamanaka, K., Koistinaho, J., Latz, E., Halle, A., Petzold, G.C., Town, T., Morgan, D., Shinohara, M.L., Perry, V.H., Holmes, C., Bazan, N.G., Brooks, D.J., Hunot, S., Joseph, B., Deigendesch, N., Garaschuk, O., Boddeke, E., Dinarello, C.A., Breitner, J.C., Cole, G.M., Golenbock, D.T., Kummer, M.P., 2015. Neuroinflammation in Alzheimer's disease. Lancet Neurol. 14, 388–405.
Hirsch, S., Guo, J., Reiter, R., Papazoglou, S., Kroencke, T., Braun, J., Sack, I., 2014. MR elastography of the liver and the spleen using a piezoelectric driver, single-shot wave-field acquisition, and multifrequency dual parameter reconstruction. Magn. Reson. Med. 71, 267–277.
Holmes, C., 2013. Review: systemic inflammation and Alzheimer's disease. Neuropathol. Appl. Neurobiol. 39, 51–68.
Huston 3rd, J., Murphy, M.C., Boeve, B.F., Fattahi, N., Arani, A., Glaser, K.J., Manduca, A., Jones, D.T., Ehman, R.L., 2016. Magnetic resonance elastography of frontotemporal dementia. J. Magn. Reson. Imaging 43, 474–478.
Jack Jr., C.R., Knopman, D.S., Jagust, W.J., Shaw, L.M., Aisen, P.S., Weiner, M.W., Petersen, R.C., Trojanowski, J.Q., 2010. Hypothetical model of dynamic biomarkers of the Alzheimer's pathological cascade. Lancet Neurol. 9, 119–128.
Johnson, C.L., Schwarb, H., M., D.J.M., Anderson, A.T., Huesmann, G.R., Sutton, B.P., Cohen, N.J., 2016. Viscoelasticity of subcortical gray matter structures. Hum. Brain Mapp. 37, 4221–4233.
Kerti, L., Witte, A.V., Winkler, A., Grittner, U., Rujescu, D., Floel, A., 2013. Higher glucose levels associated with lower memory and reduced hippocampal microstructure. Neurology 81, 1746–1752.
Klein, C., Hain, E.G., Braun, J., Riek, K., Mueller, S., Steiner, B., Sack, I., 2014. Enhanced adult neurogenesis increases brain stiffness: in vivo magnetic resonance elastography in a mouse model of dopamine depletion. PLoS One 9, e92582.
Kruse, S.A., Rose, G.H., Glaser, K.J., Manduca, A., Felmlee, J.P., Jack Jr., C.R., Ehman, R.L., 2008. Magnetic resonance elastography of the brain. NeuroImage 39, 231–237.
Lipp, A., Trbojevic, R., Paul, F., Fehlner, A., Hirsch, S., Scheel, M., Noack, C., Braun, J., Sack, I., 2013. Cerebral magnetic resonance elastography in supranuclear palsy and idiopathic Parkinson's disease. Neuroimage Clin. 3, 381–387.
Lotjonen, J., Wolz, R., Koikkalainen, J., Julkunen, V., Thurfjell, L., Lundqvist, R., Waldemar, G., Soininen, H., Rueckert, D., Alzheimer's Disease Neuroimaging, I., 2011. Fast and robust extraction of hippocampus from MR images for diagnostics of Alzheimer's disease. NeuroImage 56, 185–196.
McKhann, G., Drachman, D., Folstein, M., Katzman, R., Price, D., Stadlan, E.M., 1984. Clinical diagnosis of Alzheimer's disease: report of the NINCDS-ADRDA Work Group under the auspices of Department of Health and Human Services Task Force on Alzheimer's disease. Neurology 34, 939–944.
McKhann, G.M., Knopman, D.S., Chertkow, H., Hyman, B.T., Jack Jr., C.R., Kawas, C.H., Klunk, W.E., Koroshetz, W.J., Manly, J.J., Mayeux, R., Mohs, R.C., Morris, J.C., Rossor, M.N., Scheltens, P., Carrillo, M.C., Thies, B., Weintraub, S., Phelps, C.H., 2011. The diagnosis of dementia due to Alzheimer's disease: recommendations from the National Institute on Aging-Alzheimer's Association workgroups on diagnostic guidelines for Alzheimer's disease. Alzheimers Dement. 7, 263–269.
Misra, C., Fan, Y., Davatzikos, C., 2009. Baseline and longitudinal patterns of brain atrophy in MCI patients, and their use in prediction of short-term conversion to AD: results from ADNI. NeuroImage 44, 1415–1422.
Munder, T., Pfeffer, A., Schreyer, S., Guo, J., Braun, J., Sack, I., Steiner, B., Klein, C., 2018. MR elastography detection of early viscoelastic response of the murine hippocampus to amyloid β accumulation and neuronal cell loss due to Alzheimer's disease. J. Magn. Reson. Imaging 47, 105–114.
Murphy, M.C., Huston 3rd, J., Jack Jr., C.R., Glaser, K.J., Manduca, A., Felmlee, J.P., Ehman, R.L., 2011. Decreased brain stiffness in Alzheimer's disease determined by magnetic resonance elastography. J. Magn. Reson. Imaging 34, 494–498.
Murphy, M.C., Curran, G.L., Glaser, K.J., Rossman, P.J., Huston 3rd, J., Poduslo, J.F., Jack Jr., C.R., Felmlee, J.P., Ehman, R.L., 2012. Magnetic resonance elastography of the brain in a mouse model of Alzheimer's disease: initial results. Magn. Reson. Imaging 30, 535–539.
Murphy, M.C., Jones, D.T., Jack Jr., C.R., Glaser, K.J., Senjem, M.L., Manduca, A., Felmlee, J.P., Carter, R.E., Ehman, R.L., Huston 3rd, J., 2016. Regional brain stiffness changes across the Alzheimer's disease spectrum. Neuroimage Clin. 10, 283–290.
Muthupillai, R., Lomas, D.J., Rossman, P.J., Greenleaf, J.F., Manduca, A., Ehman, R.L., 1995. Magnetic resonance elastography by direct visualization of propagating acoustic strain waves. Science 269, 1854–1857.
Nagy, Z., Esiri, M.M., Hindley, N.J., Joachim, C., Morris, J.H., King, E.M., McDonald, B., Litchfield, S., Barnetson, L., Jobst, K.A., Smith, A.D., 1998. Accuracy of clinical operational diagnostic criteria for Alzheimer's disease in relation to different pathological diagnostic protocols. Dement. Geriatr. Cogn. Disord. 9, 219–226.
Palmqvist, S., Zetterberg, H., Mattsson, N., Johansson, P., Alzheimer's Disease Neuroimaging, I., Minthon, L., Blennow, K., Olsson, M., Swedish Bio, F.S.G., Hansson, O., 2015. Detailed comparison of amyloid PET and CSF biomarkers for identifying early Alzheimer disease. Neurology 85, 1240–1249.
Raz, N., Lindenberger, U., Rodrigue, K.M., Kennedy, K.M., Head, D., Williamson, A., Dahle, C., Gerstorf, D., Acker, J.D., 2005. Regional brain changes in aging healthy adults: general trends, individual differences and modifiers. Cereb. Cortex 15, 1676–1689.
Sack, I., Beierbach, B., Hamhaber, U., Klatt, D., Braun, J., 2008. Non-invasive measurement of brain viscoelasticity using magnetic resonance elastography. NMR Biomed. 21, 265–271.
Sack, I., Beierbach, B., Wuerfel, J., Klatt, D., Hamhaber, U., Papazoglou, S., Martus, P., Braun, J., 2009. The impact of aging and gender on brain viscoelasticity. NeuroImage 46, 652–657.
Sack, I., Streitberger, K.J., Krefting, D., Paul, F., Braun, J., 2011. The influence of physiological aging and atrophy on brain viscoelastic properties in humans. PLoS One 6, e23451.
Sack, I., Johrens, K., Wurfel, J., Braun, J., 2013. Structure-sensitive elastography: on the viscoelastic powerlaw behavior of in vivo human tissue in health and disease. Soft Matter 9, 5672–5680.
Salminen, L.E., Conturo, T.E., Bolzenius, J.D., Cabeen, R.P., Akbudak, E., Paul, R.H., 2016. Reducing Csf partial volume effects to enhance diffusion tensor imaging metrics of brain microstructure. Technol Innov 18, 5–20.
Schregel, K., Wuerfel, E., Garteiser, P., Gemeinhardt, I., Prozorovski, T., Aktas, O., Merz, H., Petersen, D., Wuerfel, J., Sinkus, R., 2012. Demyelination reduces brain parenchymal stiffness quantified in vivo by magnetic resonance elastography. Proc. Natl. Acad. Sci. U. S. A. 109, 6650–6655.
Smith, S.M., 2002. Fast robust automated brain extraction. Hum. Brain Mapp. 17, 143–155.
Smith, S.M., Jenkinson, M., Woolrich, M.W., Beckmann, C.F., Behrens, T.E., Johansen-Berg, H., Bannister, P.R., De Luca, M., Drobnjak, I., Flitney, D.E., Niazy, R.K., Saunders, J., Vickers, J., Zhang, Y., De Stefano, N., Brady, J.M., Matthews, P.M., 2004. Advances in functional and structural MR image analysis and implementation as FSL. NeuroImage 23 (Suppl. 1), S208–219.
Sperling, R.A., Aisen, P.S., Beckett, L.A., Bennett, D.A., Craft, S., Fagan, A.M., Iwatsubo, T., Jack Jr., C.R., Kaye, J., Montine, T.J., Park, D.C., Reiman, E.M., Rowe, C.C., Siemers, E., Stern, Y., Yaffe, K., Carrillo, M.C., Thies, B., Morrison-Bogorad, M., Wagster, M.V., Phelps, C.H., 2011. Toward defining the preclinical stages of Alzheimer's disease: recommendations from the National Institute on Aging-Alzheimer's Association workgroups on diagnostic guidelines for Alzheimer's disease. Alzheimers Dement. 7, 280–292.
Squire, L.R., Zola-Morgan, S., 1991. The medial temporal lobe memory system. Science 253, 1380–1386.
Streitberger, K.J., Reiss-Zimmermann, M., Freimann, F.B., Bayerl, S., Guo, J., Arlt, F., Wuerfel, J., Braun, J., Hoffmann, K.T., Sack, I., 2014. High-resolution mechanical imaging of glioblastoma by multifrequency magnetic resonance elastography. PLoS One 9, e110588.
Streitberger, K.J., Fehlner, A., Pache, F., Lacheta, A., Papazoglou, S., Bellmann-Strobl, J., Ruprecht, K., Brandt, A., Braun, J., Sack, I., Paul, F., Wuerfel, J., 2016. Multifrequency magnetic resonance elastography of the brain reveals tissue degeneration in neuromyelitis optica spectrum disorder. Eur. Radiol. 1–10.
Teipel, S., Drzezga, A., Grothe, M.J., Barthel, H., Chetelat, G., Schuff, N., Skudlarski, P., Cavedo, E., Frisoni, G.B., Hoffmann, W., Thyrian, J.R., Fox, C., Minoshima, S., Sabri, O., Fellgiebel, A., 2015. Multimodal imaging in Alzheimer's disease: validity and usefulness for early detection. Lancet Neurol. 14, 1037–1053.
Vernooij, M.W., Ikram, M.A., Vrooman, H.A., Wielopolski, P.A., Krestin, G.P., Hofman, A., Niessen, W.J., Van der Lugt, A., Breteler, M.M., 2009. White matter microstructural integrity and cognitive function in a general elderly population. Arch. Gen. Psychiatry 66, 545–553.
Wuerfel, J., Paul, F., Beierbach, B., Hamhaber, U., Klatt, D., Papazoglou, S., Zipp, F., Martus, P., Braun, J., Sack, I., 2010. MR-elastography reveals degradation of tissue integrity in multiple sclerosis. NeuroImage 49, 2520–2525.
Yakushev, I., Muller, M.J., Lorscheider, M., Schermuly, I., Weibrich, C., Dellani, P.R., Hammers, A., Stoeter, P., Fellgiebel, A., 2010. Increased hippocampal head diffusivity predicts impaired episodic memory performance in early Alzheimer's disease. Neuropsychologia 48, 1447–1453.